

Original Article

# *C. elegans* Presenilin Mediates Inter-Organelle Contacts and Communication that Is Required for Lysosome Activity

Kerry C. Ryan<sup>1</sup>, Zahra Ashkavand<sup>1</sup>, Jocelyn T. Laboy<sup>1</sup>, Ling Wang<sup>2</sup>, Margarida Barroso<sup>2</sup>, Kenneth R. Norman<sup>1\*</sup>

<sup>1</sup>Department of Regenerative and Cancer Cell Biology, <sup>2</sup>Department of Molecular Cellular Physiology, Albany Medical College, Albany, New York 12208 USA

[Received January 30, 2024; Revised February 27, 2024; Accepted February 28, 2024]

**ABSTRACT:** Compromised lysosome function is implicated in the pathology of many neurodegenerative diseases, including Alzheimer's disease (AD). Familial Alzheimer's disease (fAD) is caused primarily by mutations in the presenilin encoding genes, but the underlying mechanism remains obscure. Loss of the conserved *C. elegans* presenilin orthologue SEL-12 results in increased mitochondrial calcium, which promotes neurodegeneration. Here, we find that *sel-12* mutant lysosomes, independent of SEL-12 proteolytic activity, are significantly enlarged and more alkaline due to increased ER-to-mitochondrial calcium signaling and concomitant mitochondrial oxidative stress. These defects and their dependence on mitochondrial calcium are recapitulated in human fAD fibroblasts, demonstrating a conserved role for mitochondrial calcium in presenilin-mediated lysosome dysfunction. *sel-12* mutants also have increased contact surface area between the ER, mitochondria, and lysosomes, suggesting *sel-12* has an additional role in modulating organelle contact and communication. Overall, we demonstrate that SEL-12 maintains lysosome acidity and lysosome health by controlling ER-to-mitochondrial calcium signaling.

**Key words:** *C. elegans*, Mitochondria, Lysosomes, Calcium, Presenilin

## INTRODUCTION

The autophagy-lysosome system is a major pathway for degrading and recycling misfolded proteins and damaged organelles. Neurons rely on the autophagy-lysosome system for the preservation of protein homeostasis (proteostasis) [1, 2]. In fact, most neurodegenerative diseases are characterized by protein misfolding and aggregation indicative of a loss of proteostasis and defects in proteostasis machinery. Many studies in Alzheimer's disease (AD) neurons and AD models show disrupted autophagy, either due to deficient autophagy induction or in defective clearance of autophagosomes by the lysosomes [3, 4]. Failure to successfully clear degradative contents has severe consequences, including A $\beta$  and tau aggregation and cell death [5-7].

Familial Alzheimer's disease (fAD) is predominantly caused by mutations in the presenilin-encoding genes. Presenilins are ubiquitously expressed proteins that are phylogenetically conserved and are found in multicellular organisms, including plants, invertebrates and mammals. Additionally, presenilins are largely found on endomembrane structures and form the catalytic core of the gamma secretase complex. Presenilin is linked to AD through its ability to cleave the amyloid precursor protein to generate Abeta peptides. However, presenilin also plays important roles independent of its protease activity, including in intracellular calcium flux, lipid metabolism, and autophagy [8-15]. Indeed, fAD presenilin mutations are associated with autophagy defects at multiple stages in the process including initiation, autophagosome maturation, autophagosome fusion with lysosomes, and cargo degradation by the lysosomes [16]. Consistently,

\*Correspondence should be addressed to: Dr. Kenneth R Norman, Department of Regenerative and Cancer Biology, Albany Medical College, 47 New Scotland Avenue, Albany, NY 12208 USA. Email. [normank@amc.edu](mailto:normank@amc.edu).

**Copyright:** © 2024 Ryan KC. et al. This is an open-access article distributed under the terms of the [Creative Commons Attribution License](https://creativecommons.org/licenses/by/4.0/), which permits unrestricted use, distribution, and reproduction in any medium, provided the original author and source are credited.

we have reported that loss of the *C. elegans* presenilin 1 orthologue SEL-12 results in a loss of proteostasis [17] and disrupts autophagy [18]. In addition, we found that the proteostasis defects observed in *sel-12* mutants were dependent upon an aberrant elevation in mitochondrial calcium levels [17, 18]. There is also evidence that presenilin is necessary for proper lysosome function [10, 11, 19–22]. Lysosome morphological abnormalities are present both in presenilin FAD models and in biopsy specimens taken from AD patients [20, 23–25], suggesting lysosome dysfunction is a common feature of AD and a central aspect of AD pathology requiring further study.

Here, due to its genetic amenability and optical clarity, we use the simple in vivo model organism *C. elegans* to identify lysosomal defects in *sel-12* mutants and implicate *sel-12*-mediated calcium mitochondrial homeostasis in lysosome function. We find that the lysosomes in *sel-12* null mutants are significantly enlarged and more alkaline compared to wild type animals. Furthermore, in both *sel-12* mutants and FAD patient cells, lysosomal defects arise from elevated ER-to-mitochondria calcium signaling. Additionally, we report that loss of SEL-12 results in increased inter-organellar contacts between the ER, mitochondria, and the lysosome, suggesting that SEL-12 plays a role in regulating inter-organellar communication. Overall, these data highlight the interdependent nature of organelles and the critical role of presenilin in regulating inter-organellar contact and communication that is important for mitochondrial calcium homeostasis and lysosome function.

## MATERIALS AND METHODS

### *C. elegans* maintenance

All *C. elegans* strains were grown at 20°C on nematode growth media (NGM) plates seeded with *E. coli* OP50 unless otherwise indicated. All animals were age synchronized by bleaching gravid worms to obtain the eggs, which were then incubated in M9 for 24–48 h before being allowed to hatch. Afterward, L1 larvae were grown to adulthood on NGM plates for further experiments. Day 1 adults were analyzed for all experiments unless otherwise indicated. Genotypes were determined by PCR and DNA sequencing. The following strains were used in the study: N2 Bristol wild type, *sel-12(ar131, ok2078, tak-10, ty11)* X, *mcu-1(tm6026)* IV, *jsIs609 [mec-4p::MLS::GFP]*, *juSi271 I (col-19p::mito::dendra2)*, *pwSi82 (phyp-7-VITss::oxGFP-KDEL)*, *qxIs257 (ced-1p::nuc-1::Cherry)*, *qxIs750 (hsp::nuc-1::pHTomato)*, *takEx541 (sel-12p::sel-12::GFP)*, *takEx699 (mec-7p::lmp-1::wrmScarlet)*, *takEx767 (semo-1p::2xMLS::GCaMP6f::SL2::wrmScarlet)*, *takEx770 (semo-1p::hsp-*

*4ss::wrmScarlet::KDEL)*, *hpEx2216 (rgef-1p::mCherry::SP12)*, and *zdis5 [mec-4p::GFP]*.

### Cell lines

FAD (AG06840 and AG08170) and control (AG07621) human skin fibroblast cell lines were obtained from NIA Aging Cell Culture Repository (Coriell, Camden, NJ). AmpFLSTR Identifier Plus PCR Amplification Kit (ThermoFisher Scientific Cat#4427368) was used to authenticate the cell lines and MycoSEQ Mycoplasma Detection System (Life Technologies Cat#NC1980761) by Coriell Cell Repositories was used to test absence of mycoplasma. Cell culture media and reagents were purchased from Invitrogen (Waltham, MA) and Corning (Cellgro, Manassas, VA). All cell lines were grown in Dulbecco's modified Eagle's medium (DMEM)(Cat# 11965092) at 37°C under humidified air containing 5% CO<sub>2</sub>. The DMEM (4.5 mg/L glucose, 110 mg/L sodium pyruvate) was supplemented with penicillin (100 U/ml) (Cat#15240062), streptomycin (100 µg/ml), and 15% fetal bovine serum. Cells were cultured according to the protocol provided by the cell supplier.

### DNA constructs and transgenesis

To create the *semo-1p::secretory sequence (ss)::wrmScarlet::KDEL (takEx770)* construct, 3 kb of the 5' untranslated region of *semo-1* and *ss::wrmScarlet::KDEL* were synthesized by GenScript and combined using Gibson assembly (NEB Cat# E5510). For *takEx767 (semo-1p::2xMLS::GCaMP6f::SL2::wrmScarlet)*, the *semo-1* promoter and *wrmScarlet* were combined with *2xMLS::GCaMP6f::SL2* (amplified from pJL73) using Gibson Assembly (NEB). For *takEx699 (mec-7p::lmp-1::wrmScarlet)*, the *lmp-1* cDNA and *wrmScarlet* were synthesized by GenScript and the *mec-7* promoter was obtained from pPD46.41 (Fire Lab Vector Kit) and were combined using Gibson Assembly (NEB).

In brief, primers were designed to amplify the 5' end containing the adjacent DNA fragment and the fragment at the 3' end that will anneal to the target sequence. This creates overlapped regions at the 5' end of the primers. The Gibson Assembly reaction contains an exonuclease that creates single-strand overhang regions that will then anneal with the adjacent DNA fragment. After ligation, the product was transformed in MAX Efficiency DH5 alpha competent cells (Invitrogen), and the final construct was verified by DNA sequencing. The constructs were injected into N2 wild-type worms using standard procedures [26], along with a *ttx-3p::GFP* co-injection fluorescent marker that labels the bilaterally symmetrical AIY neurons (gift from O. Hobert, Columbia University).

Fluorescent microscopy was used to confirm the correct subcellular localization of all constructs.

### RNAi treatments

RNAi was delivered by feeding as described [27]. L1 animals were grown to day 1 of adulthood on NGM plates seeded with HT115 *E. coli* bacteria that produced either empty feeding vector, or *itr-1* or *unc-68* double-stranded RNA. These bacteria were obtained from the Ahringer library [28] and production of *itr-1* and *unc-68* was verified by PCR. Day 1 adult animals were analyzed.

### Calcium imaging

Mitochondrial calcium concentration was measured in the *C. elegans* hypodermis in animals expressing *semo-1p::2xMLS::GCaMP6f::SL2::wrmScarlet*. Animals were first immobilized on slides using 500mM levamisole on 2% agarose pads. Images of the animals were captured using a 63x objective lens on a Zeiss Axio Observer microscope equipped with an Andor Clara CCD camera. The ratio of GCaMP6f::SL2::wrmScarlet fluorescence intensity was quantified so that GCaMP6f fluorescence was normalized to wrmScarlet intensity. Metamorph software was used to compile images.

### Drug treatments

N-acetyl cysteine (NAC) (Sigma-Aldrich, Cat#A7250) was prepared in DMSO and added to NGM plate media at 9 mM, and animals were moved to NAC plates as L4 animals until adulthood, as previously described [17]. For mitoTEMPO experiments, either 500  $\mu$ M of (2-(2,2,6,6-tetramethylpiperidin-1-oxyl-4-ylamino) -2-oxoethyl) triphenylphosphonium chloride (mitoTEMPO) (Sigma-Aldrich Cat# SML0737) or 500  $\mu$ M triphenylphosphonium chloride (TPP) (Sigma-Aldrich Cat# 11726LE) was added to NGM plates. Animals were moved to mitoTEMPO or TPP plates as L1 larvae.

### Quantification of lysosome volume and acidity

Lysosomes were imaged in transgenic animals expressing NUC-1::CHERRY driven by the ubiquitous *ced-1* promoter (*qxIs257*). These animals were co-expressing *mec-4p::GFP* (*zdl5*) to mark the touch receptor neurons; lysosomes present within the GFP signal were identified as touch receptor neuron lysosomes. All images were captured at 60 $\times$  magnification using a Nikon laser-scanning confocal microscope with NIS Elements software, with z-stacks acquired at 0.25  $\mu$ m slice intervals. For hypodermis lysosomes, a selection of lysosomes at the midbody of the worm was analyzed and

lysosome volume was averaged for each worm. Volume was quantified using Imaris 9.0 software. 20 animals per strain were analyzed.

To compare the relative pH between strains, we examined animals expressing NUC-1::pHTomato, where pHTomato is a pH-sensitive fluorescent protein. This construct is driven under the heat shock promoter. To induce expression, animals were heat shocked at 37°C for 30 minutes, then incubated at 20°C for 24 hours so that the transgenic protein could enter the lysosome [29]. Images of the lysosomes in the hypodermis were taken at 60 $\times$  magnification using a Nikon laser-scanning confocal microscope with NIS Elements software, with z stacks acquired at 0.25  $\mu$ m slice intervals. All settings for pinhole size and laser power were identical for all images taken. Imaris 9.0 software was used to quantify the mean fluorescent intensity of each lysosome. 20 animals per strain were analyzed.

### Lysosome volume measurements in FAD fibroblasts

To image fibroblast lysosomes, live cells were plated onto 35mm glass bottom dishes (MatTek Corp) and left to attach overnight. The following day, the cells were either incubated for 1 hour with 100nM LysoTracker red DND99 dye (Invitrogen Cat# L7528) or labeled with Celllight™ Lysosomes RFP BacMam 2.0 (Invitrogen Cat# C10597) overnight at 37°C. Cells were imaged immediately following incubation using confocal microscopy. For Ru265 treatment, fibroblasts were treated with 10  $\mu$ M Ru265 (Calbiochem) for 48 hr. Imaris 9.0 software was used to quantify lysosome volume, and at least 20 cells were imaged per line.

### Inter-organelle contact surface area

To measure mitochondria-lysosome contacts within the hypodermis, transgenic animals were generated co-expressing *qxIs257* (*ced-1p::NUC-1::Cherry*) to mark the lysosomes and *juSi271 I* (*col-19p::mito::dendra2*) to mark the mitochondria. Similarly, lysosome-ER contacts were measured in animals co-expressing an ER marker [*pwSi82* (*phyp-7-VITss::oxGFP-KDEL*)] and lysosome marker (*qxIs257*), and ER-mitochondria contacts were measured in animals co-expressing *juSi271* and *takEx770* (*semo-1p::wrmScarlet::KDEL*). Animals were immobilized on slides using 500mM levamisole on 2% agarose pads. All images were captured at 60 $\times$  magnification using a Nikon laser-scanning confocal microscope with NIS Elements software, with z-stacks acquired at 0.25  $\mu$ m slice intervals through the depth of the hypodermis. Images were taken at the midbody of each animal. Colocalization analysis was performed on Imaris 9.0 using the XTension “Surface Contact Area”

Imaris plugin (<https://imaris.oxinst.com/open/view/surface-surfacecontact-area>), as described previously [30], with the “surface” module used to create a 3D rendering of organelle surfaces, and background subtraction held constant within an experiment. The ratio of contact surface area: total surface area was determined by summing the contact area within the field of view and dividing by the area of the hypodermis within the field of view. 20 animals per strain were analyzed.

### Quantification and statistical analysis

Statistical difference comparing two treatment groups was determined using a Student's t test, and for parametric data, a one-way analysis of variance with a Tukey post hoc analysis was used for multiple comparisons. Normal distribution of these data was determined using the Shapiro-Wilk test. For non-parametric data, Kruskal-Wallis test with Dunn's post hoc analysis was used. For the coelomocyte morphology analysis, a chi-square test was used to determine statistical difference between genotypes. A p value of less than 0.05 was considered significant. Graph Pad Prism software was used for all statistical analyses.

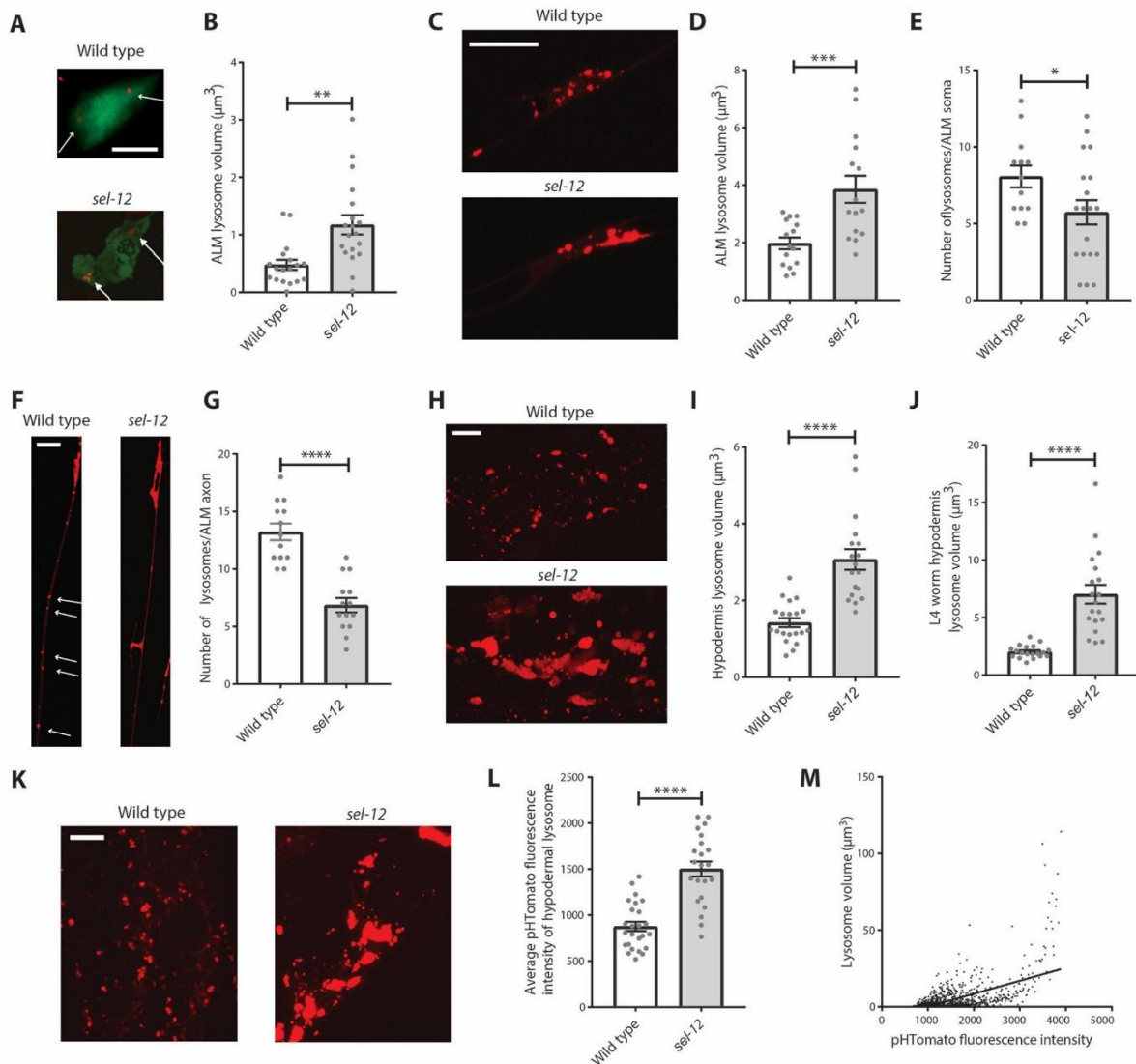


**Figure 1. *sel-12* mutant lysosomes are enlarged and more alkaline.** (A) Representative images of wild type and *sel-12(ty11)* lysosomes within the ALM soma in animals co-expressing *nuc-1::mCherry* as a marker for lysosomes (arrows) and *mec-4p::GFP* to mark the TRNs (scale bar = 5  $\mu$ m). (B) Quantification of average lysosome volume within the ALM TRN soma in wild type and *sel-12* animals ( $n \geq 18$  animals). (C and D) Representative images of wild type and *sel-12(ty11)* lysosomes in the ALM soma in animals expressing *mec-7p::lmp-1::wrmScarlet* (C) (scale bar = 5  $\mu$ m), and quantification of average lysosome volume (D) ( $n \geq 18$  animals). (E) Quantification of the number of lysosomes per soma in animals expressing *mec-7p::lmp-1::wrmScarlet* ( $n \geq 14$  animals). (F and G) Representative images of wild type and *sel-12* lysosomes (arrows) in the axons of animals expressing *mec-7p::lmp-1::wrmScarlet* (scale bar = 5  $\mu$ m) (F) and quantification of the number of *lmp-1::wrmScarlet* puncta per ALM axon (G) ( $n \geq 13$ ). (H and I) Representative images of hypodermal



lysosomes in animals expressing *nuc-1::mCherry* as a marker for the lysosomal lumen (scale bar = 10  $\mu$ m) (**H**) and quantification of average hypodermal lysosome volume (**I**) ( $n \geq 18$  animals). (**J**) Lysosome volume (*nuc-1::mCherry*) in L4 wild type and *sel-12* animals ( $n \geq 19$  animals). (**K and L**) Representative images (**K**) and quantification of the average pHTomato fluorescence intensity per lysosome in animals expressing *nuc-1::pHTomato* controlled by the heat-shock promoter (**L**) (scale bar = 10  $\mu$ m) ( $n \geq 21$  animals). Increased pHTomato fluorescence intensity indicates increased pH. (**M**) Linear regression for pHTomato fluorescence volume and intensity in *sel-12(ty11)* mutants ( $p < 0.001$ ). ns  $p > 0.05$ , \*  $p < 0.05$ , \*\*  $p < 0.01$ , \*\*\*  $p < 0.001$ , \*\*\*\*  $p < 0.0001$ . For D, G, I, J, and L, a two-tailed Student's *t* test was used. For B and E, Kruskal-Wallis test was used. Error bars indicate mean  $\pm$  SEM.

## RESULTS

### *sel-12* mutants display abnormal lysosome morphology and impaired lysosomal function

There is evidence that presenilin plays an important role in lysosome function [22] [4, 12], but the underlying mechanism is unclear. The lysosomes in *C. elegans sel-12* mutants have not yet been characterized. Therefore, we first examined lysosome morphology and distribution in the touch receptor neurons (TRNs). The TRNs undergo stereotyped age-associated neurodegeneration [31, 32] and this occurs prematurely in *sel-12* mutants [13]. We utilized transgenic animals expressing TRN-specific soluble GFP [33] and mCherry tagged NUC-1 [29], a lysosomal nuclease and a marker for the lysosomal lumen [34]. TRN lysosomes, visualized as small puncta in day 1 adult animals, were distinguished by the colocalization of GFP and mCherry markers in neuronal cell bodies (Fig. 1A). We introduced these markers into three *sel-12* mutants: *sel-12(ty11)*, which contains a premature stop codon in *sel-12* that leads to a predicted truncated protein and null mutant [35]; *sel-12(ar131)*, which contains a missense mutation that is conserved with an fAD-linked presenilin mutation [36]; and *sel-12(ok2078)*, a deletion mutant [17]. We found a significant increase in lysosome volume in the *sel-12* mutant TRNs (Fig. 1A, B, S1A). As an additional strategy for visualizing TRN lysosomes, we expressed wrmScarlet [37] tagged to the lysosome-associated membrane protein 1 (LAMP1) driven under a TRN-specific promoter. Similarly, we found that while wild type animals showed small evenly sized lysosomes, the lysosomes in the *sel-12* mutants were significantly enlarged (Fig. 1C, D). We also found that *sel-12* mutants had a significant reduction in the number of lysosomes within their ALM soma (Fig. 1E) and axons (Fig. 1F, G). To examine lysosome characteristics in more detail, we looked at the lysosomes in the hypodermis; since the hypodermis is one of the largest tissues in *C. elegans*, lysosomes are easily visualized. In addition, the hypodermis, like most *C. elegans* tissues, is post-mitotic so it recapitulates the reliance of neurons upon the autophagy-lysosome system. Examining the *C. elegans* hypodermis therefore allows more detailed analyses of lysosomes in a cell that shares a sensitivity to lysosome dysfunction. To examine lysosomes in the hypodermis,

we introduced a NUC-1::mCherry transgene driven under a ubiquitous promoter into the *sel-12* mutant background [29]. Consistent with our analyses of the TRNs, we found that *sel-12* animals also had enlarged lysosomes in the hypodermis (Fig. 1H, I, Supplementary Fig. 1B).

We previously found that neuronal and behavioral defects in *sel-12* mutants do not appear prior to adulthood. Indeed, *sel-12* mutants at the L4 larval stage, the stage prior to adulthood, are phenotypically wild type [13]. We examined whether the abnormal lysosome morphology precedes neuronal dysfunction and found that L4 *sel-12* mutants have enlarged lysosomes compared to L4 wild type animals (Fig. 1J). This indicates that aberrant lysosome morphology occurs prior to major signs of neurodegeneration and may indicate a causal relationship between lysosome defects and neurodegeneration. Notably, enlarged hypodermal lysosomes have been observed in aged animals [29], suggesting premature lysosomal dysfunction in *sel-12* mutants.

Next, we asked whether the lysosome morphological abnormalities indicated lysosome dysfunction. To accomplish this, we measured relative lysosome pH by examining animals transiently expressing NUC-1 fused with the pH sensitive fluorescent protein pHTomato using a heat shock inducible promoter [29]. pHTomato's emission intensity is highly pH-dependent, and increases with higher pH [38]. By comparing pHTomato fluorescence intensity between wild type and *sel-12* mutants, we found that *sel-12* mutants had a significantly higher pHTomato fluorescence intensity, indicating that *sel-12* mutant lysosomes are more alkaline, demonstrating lysosomal dysfunction (Fig. 1K, L, S1C). Lysosome volume also correlated with pHTomato fluorescence intensity, suggesting that lysosomal enlargement is associated with impaired lysosome function (Fig. 1M). Overall, we found that *sel-12* mutants have significant lysosome morphological and functional defects, consistent with other studies on lysosomal biology in other AD and presenilin fAD models [20, 22–24, 39].

### Abnormal lysosome morphology is independent of gamma-secretase proteolytic activity in *sel-12* mutants

To explore causes of lysosome enlargement, we examined whether lysosome morphology defects in *sel-12* mutants are the result of SEL-12's proteolytic function. SEL-12,

like mammalian presenilin, is the proteolytic subunit of the gamma secretase complex, which is responsible for cleaving the Notch receptor and other type I integral membrane proteins. Presenilin/gamma secretase is associated with fAD via its role in processing Abeta peptides, but there is also evidence that presenilin additionally contributes to fAD pathology through alternate gamma-secretase-independent mechanisms [8-13, 15]. To determine whether the lysosome morphology in *sel-12* mutants is impacted by *sel-12* protease activity, we examined the lysosomes in a *sel-12* CRISPR/Cas9

engineered mutant that contains a D to A mutation within the endogenous *sel-12* gene that codes for a residue necessary for its aspartyl-protease activity, D226A, and which we have previously verified abolishes gamma secretase function [17]. Hypodermal lysosome volume in *sel-12(D226A)* mutants was not significantly different from wild type animals, while it was significantly smaller compared to *sel-12* mutant lysosomes (Supplementary Fig. 1D), indicating that SEL-12's impact on the lysosome is gamma-secretase independent.

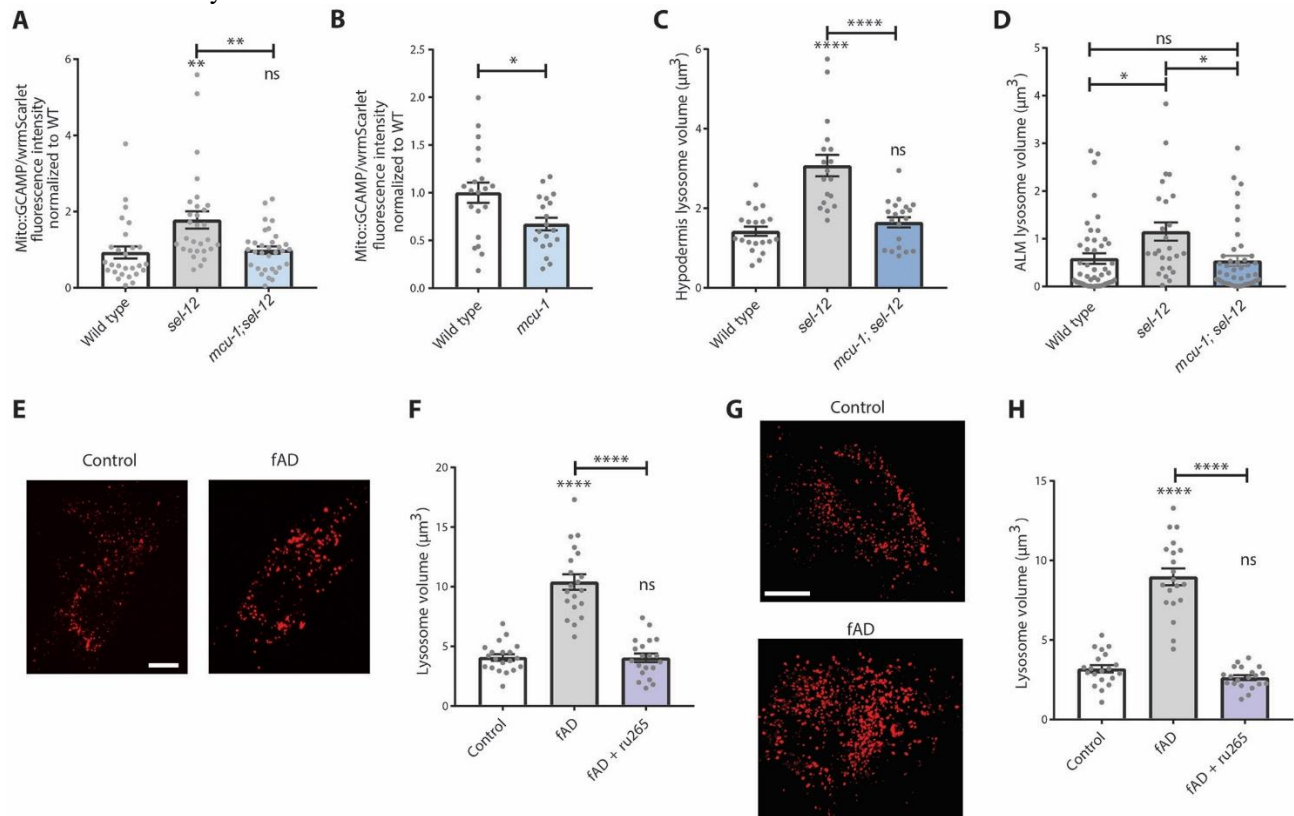


**Figure 2. *sel-12*-mediated lysosome dysfunction is ameliorated by blocking mitochondrial calcium uptake.** (A and B) Fluorescence intensity of mitochondrial-targeted GCaMP6, a genetically encoded calcium indicator, in the hypodermis of animals also expressing cytosolic wrmScarlet as an internal expression control (*semo-1p::2xMLS::GCaMP6f::SL2::wrmScarlet*). (C) Quantification of hypodermal lysosome volume in wild type, *sel-12*, and *mcu-1; sel-12* animals expressing *nuc-1::mCherry* as a marker for the lysosomal lumen ( $n \geq 18$  animals). (D) Lysosome volume within the ALM soma in animals co-expressing *nuc-1::mCherry* to mark the lysosomes and *mec-4p::GFP* to mark the TRNs ( $n \geq 18$  animals). (E and F) Representative images of lysotracker-labeled lysosomes in fibroblasts isolated from control and fAD patients (scale bar = 15  $\mu\text{m}$ ) and (F) quantification of lysosome volume (+/- ru265) ( $n = 20$  cells). (G and H) Representative images of lysosomes in control and fAD patient fibroblasts transfected with Lamp1-RFP (Celllight BacMam 2.0, Invitrogen) (scale bar = 20  $\mu\text{m}$ ), and (H) quantification of lysosome volume (+/- ru265) ( $n = 20$  animals). ns  $p > 0.05$ , \*  $p < 0.05$ , \*\*  $p < 0.01$ , \*\*\*  $p < 0.001$ , \*\*\*\*  $p < 0.0001$ . For B, C, F, and H, one-way ANOVA with Tukey's multiple comparisons test was used. For A and D, Kruskal-Wallis test with Dunn's multiple comparison test was used. Error bars indicate mean  $\pm$  SEM. Comparisons are made to wild type unless otherwise indicated.

### Lysosome abnormalities are suppressed by reducing mitochondrial calcium uptake

We previously determined that aberrant mitochondrial calcium homeostasis contributes to neurodegeneration in *sel-12* mutants [13, 17]. Therefore, we wished to establish

the connection between mitochondrial calcium, lysosome dysfunction, and neurodegeneration. To determine whether mitochondrial calcium causes lysosome enlargement and dysfunction, we first asked whether mitochondrial calcium is elevated in the *sel-12* hypodermis as it is in the neurons [13]. We expressed a

mitochondrial targeted GCaMP calcium sensor, driven under a hypodermal-specific promoter, co-expressing a wrmScarlet marker as an expression control. We found calcium levels were elevated in hypodermal mitochondria in *sel-12* mutants (Fig. 2A). Additionally, using a mitochondrial-targeted GFP driven by a hypodermis-specific promoter, we found the hypodermal mitochondrial network is disorganized and fractured (Supplementary Fig. 2). These data are consistent with previous results in *sel-12* neurons, where elevated calcium levels correlated with mitochondrial morphological defects [13]. To confirm whether increased mitochondrial calcium uptake in the hypodermis is responsible for the fractured mitochondrial network, we suppressed

mitochondrial calcium uptake in *sel-12* mutants with a mitochondrial calcium uniporter (*mcu-1*) null mutation, which we and others have shown reduces mitochondrial calcium levels (Fig. 2B)[13, 40, 41]. Introducing the *mcu-1* mutation into the *sel-12* mutant background prevented the increased mitochondrial calcium levels (Fig. 2A) and mitochondrial network fragmentation (Supplementary Fig. 2), indicating elevated mitochondrial calcium uptake in the hypodermis following SEL-12 loss causes mitochondrial disorganization and morphological changes (Supplementary Fig. 2). This also provides evidence that the hypodermis mimics the aberrant calcium signaling present in *sel-12* mutant neurons and the resulting mitochondrial abnormalities [13].

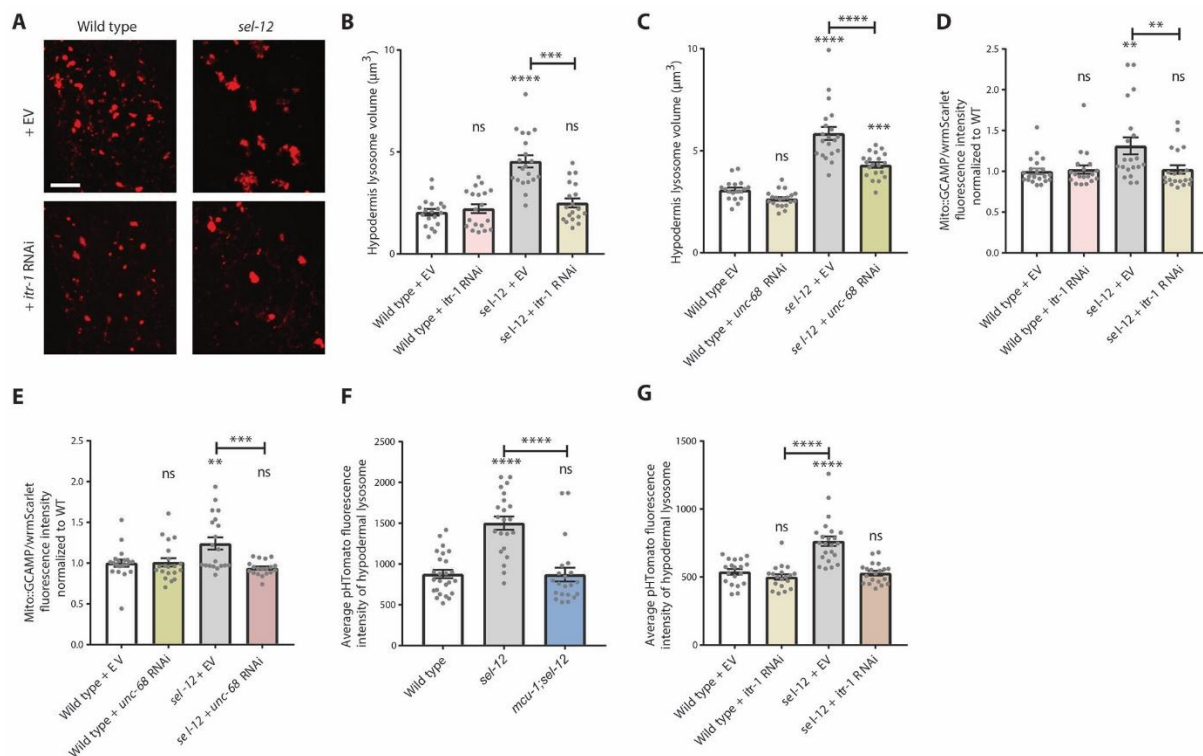


**Figure 3. Aberrant ER-to-mitochondrial calcium transfer results in enlarged, more alkaline lysosomes. (A and B)** Representative images of lysosomes (*nuc-1::mCherry*) in wild type and *sel-12(ty11)* animals grown on either control empty vector (EV) or *itr-1* RNAi (A) (scale bar = 10  $\mu$ m), and quantification of lysosome volume (B) ( $n \geq 19$  animals). (C) Quantification of lysosome volume (*nuc-1::mCherry*) in animals grown on either EV or *unc-68* RNAi ( $n \geq 18$  animals). (D and E) Fluorescence intensity of hypodermal mitochondrial-targeted GCaMP6, a genetically encoded calcium indicator, normalized to cytosolic wrmScarlet, used as an internal expression control ( $n \geq 19$  animals). (F) Quantification of the average pHTomato fluorescence intensity per lysosome in animals expressing *nuc-1::pHTomato* controlled by the heat-shock promoter, with increased pHTomato fluorescence intensity indicating increased pH ( $n \geq 21$  animals). (G) *nuc-1::pHTomato* fluorescence in wild type and *sel-12(ty11)* animals grown on either EV or *itr-1* RNAi ( $n \geq 19$  animals). ns  $p > 0.05$ , \*  $p < 0.05$ , \*\*\*  $p < 0.001$ , \*\*\*\*  $p < 0.0001$ . For C and G, one-way ANOVA with Tukey's multiple comparisons test was used. For B, D, E, and F, Kruskal-Wallis test with Dunn's multiple comparison test was used. Error bars indicate mean  $\pm$  SEM. Comparisons are made to wild type unless otherwise indicated.

To determine whether this increase in mitochondrial calcium also contributes to lysosomal enlargement, we compared *sel-12* mutants with *mcu-1*; *sel-12* double mutants expressing the transgenic NUC-1 lysosomal marker. We found that *mcu-1*; *sel-12* mutants had reduced

lysosome volume in both the hypodermis (Fig. 2C) and in the TRNs (Fig. 2D) and resembled wild type lysosomes, implicating increased mitochondrial calcium uptake in altered lysosome morphology.

We next asked whether the effect of mitochondrial calcium on lysosomes is conserved in human cells. Studies examining cell lines from patients that harbor fAD presenilin mutations have found enlarged lysosomes [10, 20, 24] but the cause of the enlargement remains unclear. Therefore, we first determined lysosome size in fibroblasts isolated from patients with PSEN1 fAD mutations. We have previously found evidence that the fAD fibroblasts have elevated mitochondrial calcium [13]. Using lysotracker to label live fibroblast lysosomes, we found that, like previous studies and similar to the *sel-12* mutants, fAD fibroblasts had enlarged lysosomes (Fig. 2E, F). Importantly, fAD cells treated with the mitochondrial calcium uniporter inhibitor, ruthenium 265 (ru265), showed significantly lower lysosome volume compared to untreated fAD fibroblast (Fig. 2F). Alternatively, we labeled the lysosomes by transfecting fibroblast cells with a Lamp1-RFP fusion vector. Using this method, we also found ru265 treatment rescued increased lysosome volume in fAD cells (Fig. 2G, H). Considering that previous data show mitochondrial calcium is elevated in these fAD cells [13], this suggests that this potential pathogenic mechanism is conserved in human cells.

#### Altered ER-to-mitochondrial calcium signaling mediates lysosomal morphology and functional defects

Elevated ER calcium release has been implicated in neuronal dysfunction in fAD models [42-44]. Additionally, we have previously demonstrated that impairing calcium release from the ER reduces mitochondrial calcium and prevents neuronal dysfunction in *sel-12* mutants [13]. There is also evidence of increased ER-mitochondrial contacts in fAD presenilin patient cell lines [8, 45]. Therefore, we asked whether ER calcium release contributes to the lysosomal enlargement and alkalization observed in *sel-12* mutants. To inhibit ER calcium release, we treated *sel-12* mutants with RNAi knockdown of *itr-1*, which encodes the *C. elegans* inositol 1, 4, 5-trisphosphate receptor (IP3R) orthologue. Compared to *sel-12* mutants grown on control empty vector (EV) RNAi, *itr-1(RNAi)*; *sel-12* animals had significantly reduced lysosome volume indistinguishable from those of wild type animals (Fig. 3A, B). As an alternative strategy to inhibit ER calcium release, we treated *sel-12* mutants with RNAi knockdown of *unc-68*, which encodes the *C. elegans* orthologue of the ryanodine receptor. Although not as robust as *itr-1* depletion, we found that *unc-68* RNAi treatment also reduced lysosome volume (Fig. 3C). Furthermore, both *itr-1(RNAi)* and *unc-68(RNAi)* knockdown reversed the elevation of mitochondrial calcium levels in *sel-12* mutants (Fig. 3D and E), demonstrating that blocking ER calcium release

prevents excessive mitochondrial calcium uptake. Together with the reduced lysosome volume data observed in *mcu-1*; *sel-12* animals (Fig. 2C), these data show that calcium transfer from the ER into the mitochondria impacts lysosome morphology.

Next, we also wished to determine whether ER-to-mitochondrial calcium signaling is responsible for acidification defects found in *sel-12* mutant lysosomes. We examined *nuc-1::pHTomato* fluorescence intensity after blocking ER calcium release or mitochondrial calcium uptake in *sel-12* mutants. Either *itr-1* RNAi depletion or *mcu-1* knockout in the *sel-12* mutant background improved lysosome acidity as measured by a reduction in pHTomato fluorescence (Fig. 3F, G).

Overall, these data show that altered calcium signaling between the ER and mitochondria has morphological and functional consequences on the lysosome, an organelle critical for protein and organelle homeostasis. The data demonstrates that a defect in inter-organelle communication between the ER and mitochondria impacts the morphology and function of the lysosome, signifying the interdependent nature of organelles and highlights that organelles do not act as solitary compartments.

#### *sel-12* mutants have increased mitochondria and ER contact that is dependent on inositol 1,4,5-trisphosphate receptor (ITR-1) function

fAD presenilin mutations have previously been linked with increased contact sites between the ER and the mitochondria, which increased signaling and exchange of materials between the two organelles [8, 46]. Presenilin predominantly localizes to the ER and is enriched at the region of ER membrane that is in direct contact with mitochondria [47]. In line with this, presenilin can affect ER-mitochondria calcium and lipid signaling by regulating the level of physical contact between the ER and mitochondria [8, 13, 45, 47]. It has therefore been speculated that presenilin mediates ER-mitochondrial communication, and that AD at least partially results from dysregulated inter-organelle signaling [48]. Therefore, we asked whether loss of SEL-12 recapitulated this potentially pathogenic mechanism in *sel-12* null mutants, and whether altering ER-mitochondrial calcium exchange would disrupt ER-mitochondrial contact. To first determine if SEL-12, like mammalian presenilin, localizes to the ER, we examined animals co-expressing a functional SEL-12::GFP fusion protein [13] and an ER reporter (mCherry::SP12) [49]. Similar to previous studies [50], SEL-12 showed perinuclear expression and colocalized with the ER marker, indicating SEL-12 localizes to the ER (Supplementary Fig. 3).



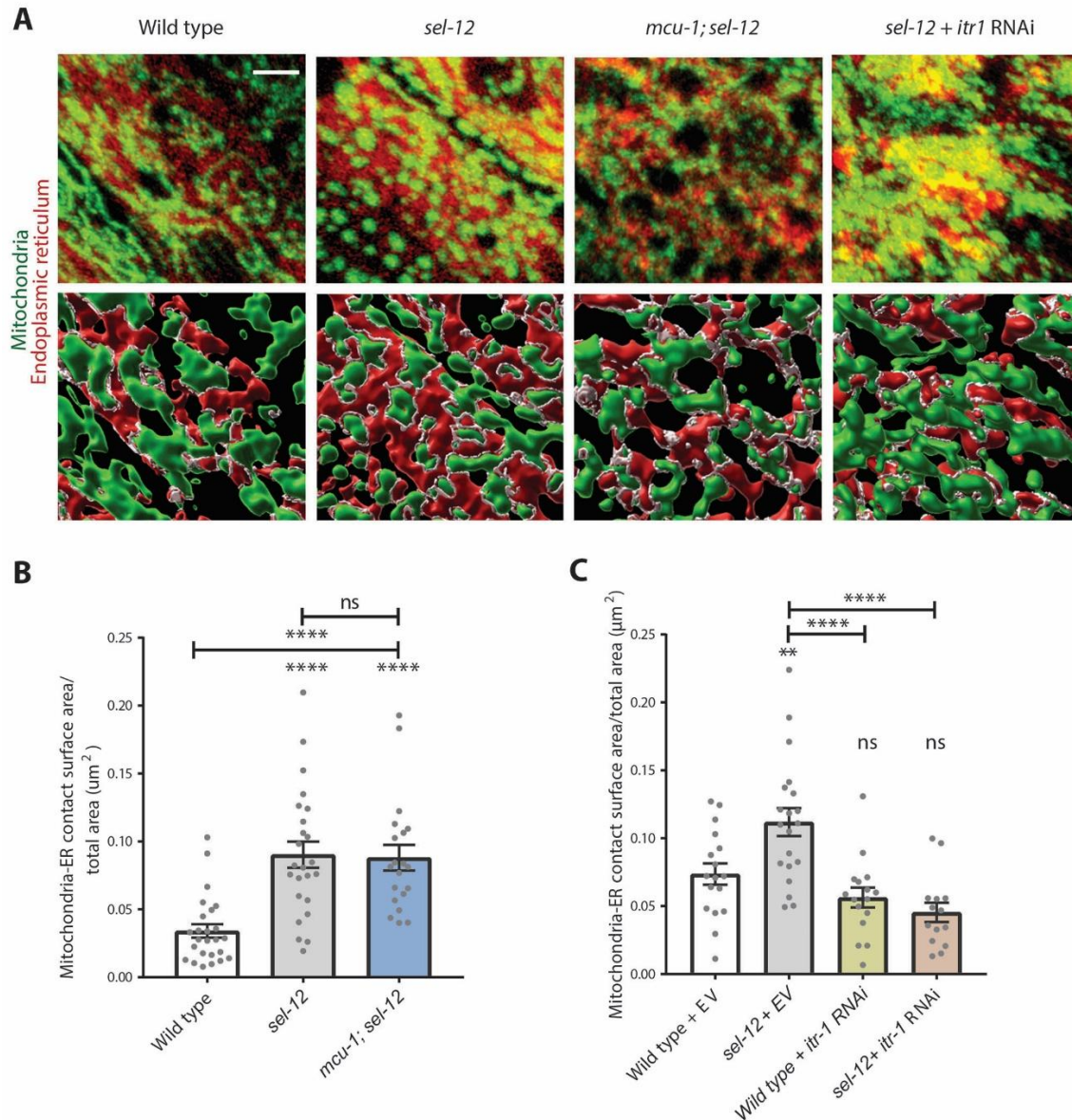


**Figure 4. *sel-12* mutants have increased mitochondria and endoplasmic reticulum contact points dependent upon *itr-1* function but not *mcu-1*.** (A) Representative confocal z-stack images of hypodermal mitochondria (green) and endoplasmic reticulum (red) and rendering of 3D images (bottom panels) with white indicating ER-mitochondrial contact points (scale bar = 4 μm). (B) Quantification of the ratio of mitochondria-ER contact surface area to total area of visible hypodermis in wild type, *sel-12*(*ty11*), and *mcu-1; sel-12*(*ty11*) animals (n ≥ 20 animals). (C) Mitochondrial-ER contact surface to total surface area ratio in animals treated with either empty vector (EV) or *itr-1* RNAi (n ≥ 15 animals). ns p > 0.05, \*p < 0.05, \*\*\*\*p < 0.0001 using Kruskal-Wallis with Dunn's post-hoc test. Error bars indicate mean ± SEM. Comparisons are made to wild type unless otherwise indicated.

To examine contacts between the ER and mitochondria, we generated transgenic animals co-expressing an ER marker (*wrmScarlet::KDEL*) and a mitochondrial marker (*mito::dendra2*) [51]. We imaged ER-mitochondrial contacts in the hypodermis at a defined region of interest at the center of the animal, and quantified organelle contacts following a previously established methodology for 3D rendering and surface contact analysis [30]. Consistent with previous studies in

presenilin FAD cell models [8, 45-47], we found that the ER-mitochondrial contact area was increased in *sel-12* mutants (Fig. 4A, B). However, inhibition of mitochondrial calcium uptake via the *mcu-1* null mutation did not alter the level of mitochondria-ER contact in *sel-12* mutants (Fig. 4A, B). This suggests that increased mitochondrial calcium is a consequence of increased ER-mitochondria contact rather than a cause. It also proposes that SEL-12 acts at the ER to influence ER-mitochondrial

connections, which promotes ER-mitochondrial calcium exchange. In contrast, depleting *itr-1* via RNAi prevented the increase in ER-mitochondrial contacts in *sel-12* mutants (Fig. 4A, C). This may indicate that either *itr-1* function in ER calcium release promotes ER-

mitochondria connections and/or the ITR-1 protein itself acts to mediate ER-mitochondrial contacts. Indeed, evidence in the literature shows inositol 1,4,5-trisphosphate receptor is critical for mediating ER-mitochondrial contact [52-54].

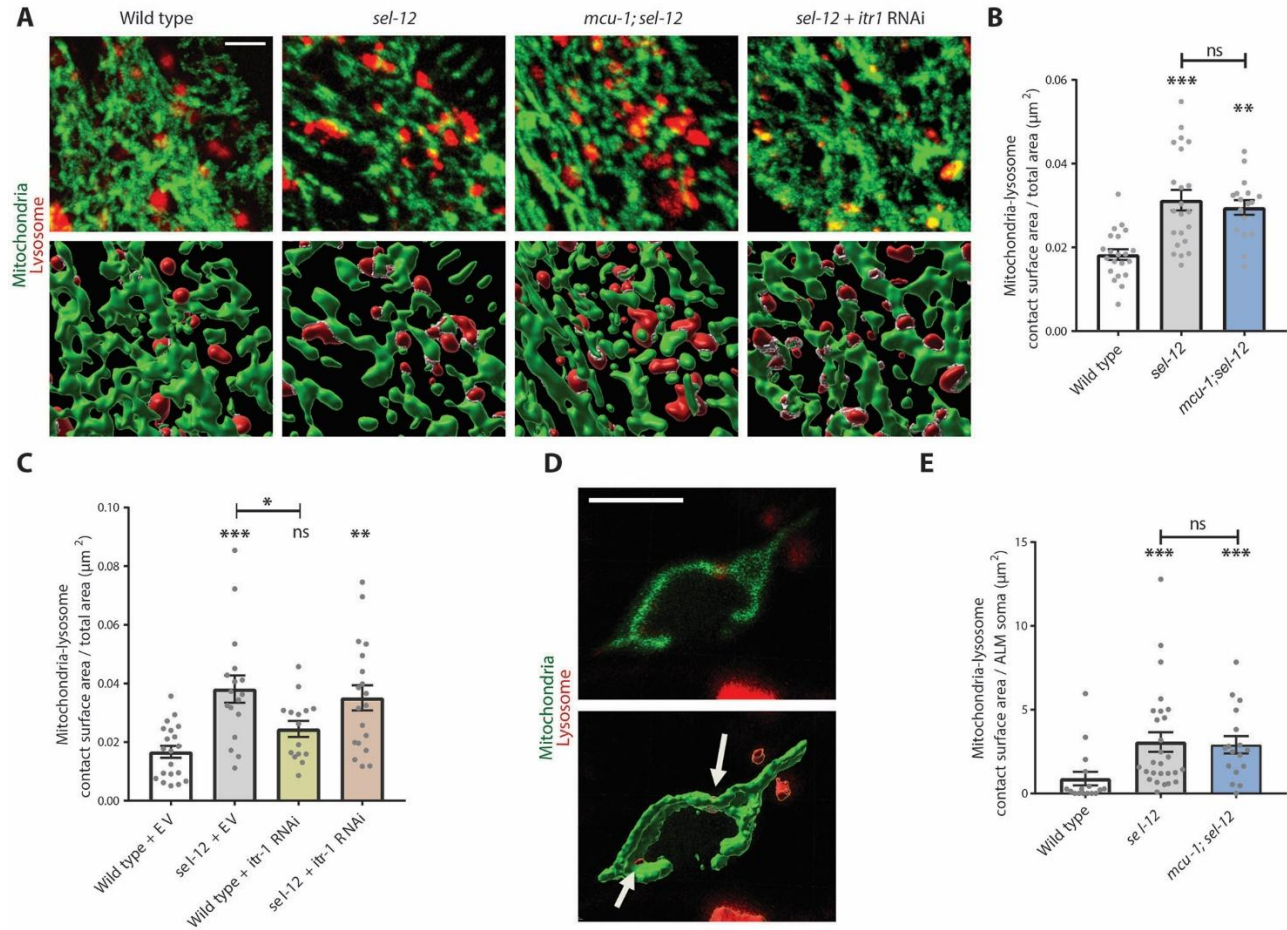


**Figure 5. *sel-12* mutants have increased mitochondria and lysosome contact points.** (A) Representative confocal z-stack images of hypodermal mitochondria (green) and lysosomes (red) (scale bar = 4 μm) and rendering of 3D images (bottom panels) with white indicating mitochondria-lysosome contact points (scale bar = 4 μm). (B) Quantification of the ratio of mitochondria-lysosome contact surface area to total area of visible hypodermis in wild type, *sel-12*(*ty11*), and *mcu-1; sel-12*(*ty11*) animals ( $n \geq 17$  animals). (C) Mitochondria-lysosome contact surface to total surface area ratio in animals treated with either empty vector or *itr-1* RNAi ( $n \geq 15$  animals). (D) Representative images of confocal z-stack (upper panel) and 3D rendered (lower panel) images of ALM soma in animals co-expressing a mitochondrial marker driven under a TRN-specific promoter and a lysosome marker, with arrows indicating contact sites between lysosomes and neuronal mitochondria (scale bar = 5 μm). (E) Quantification of mitochondria-lysosome contact surface area per ALM soma ( $n \geq 16$  animals). ns  $p > 0.05$ , \* $p < 0.05$ , \*\* $p < 0.01$ , \*\*\* $p < 0.001$ . For B and C, one-way ANOVA with Tukey's multiple comparisons test was used. For E, Kruskal-Wallis test with Dunn's multiple comparison test was used. Comparisons are to wild type unless otherwise indicated. Error bars indicate mean  $\pm$  SEM.

### Inter-organelle contacts between mitochondria-lysosomes and lysosomes-ER are increased in *sel-12* mutants

Presenilin has also been found to localize to lysosomal membranes [10, 47, 55, 56]. Therefore, loss of presenilin

may additionally influence communication between lysosomes and other organelles. Since we observed increased contacts between the mitochondria and ER, we asked whether other inter-organelle contacts were altered in *sel-12* mutants.



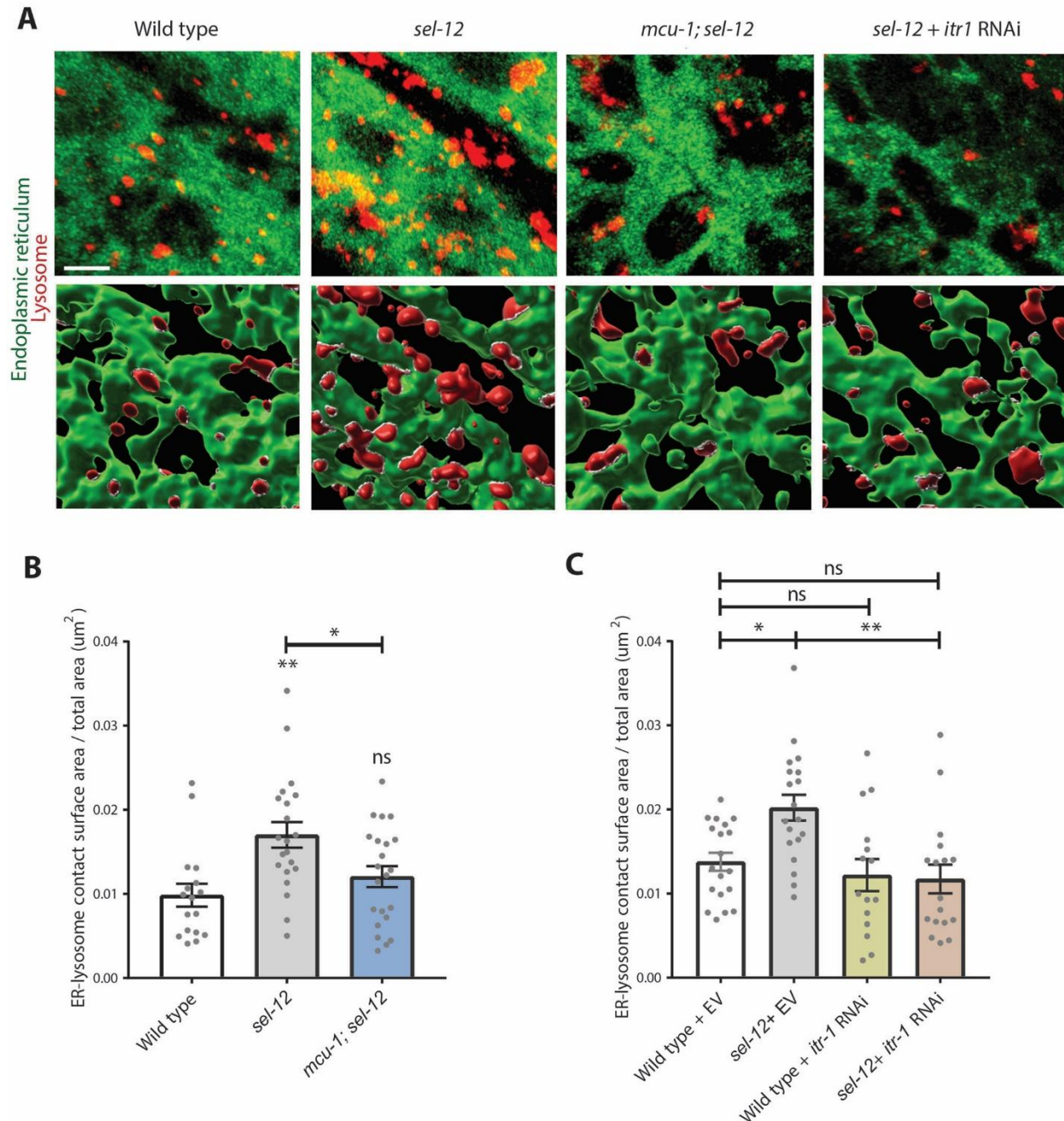


**Figure 6. *sel-12* mutants have increased endoplasmic reticulum and lysosome contact points dependent upon ER-to-mitochondria calcium signaling.** (A) Representative confocal z-stack images of hypodermal endoplasmic reticulum (green) and lysosomes (red) and rendering of 3D images (bottom panels) with white indicating ER-lysosome contact points (scale bar = 4  $\mu\text{m}$ ). (B) Quantification of the ratio of mitochondria-ER contact surface area to total area of visible hypodermis in wild type, *sel-12(ty11)*, and *mcu-1; sel-12* animals ( $n \geq 17$  animals). (C) Mitochondrial-ER contact surface to total surface area ratio in animals treated with either empty vector or *itr-1* RNAi ( $n \geq 15$  animals). ns  $p > 0.05$ , \* $p < 0.05$ , \*\* $p < 0.01$  using one-way ANOVA with Tukey's multiple comparison test. Comparisons are made to wild type unless otherwise indicated. Error bars indicate mean  $\pm$  SEM.

First, to determine whether there is evidence of increased inter-organelle contacts between the lysosomes and mitochondria, we quantified the area of contact between these two organelles. We utilized mito-Dendra2, to label mitochondria [51] and NUC-1::mCherry, to label

lysosomes [57] in the hypodermis. We found that the mitochondria and lysosomes had an increased ratio of contact surface area to total surface area of the hypodermis in the *sel-12* mutants versus wild type animals (Fig. 5A, B), indicating a greater total area of

mitochondria-lysosome contacts within the hypodermis. However, this increase was not dependent on mitochondrial calcium uptake. Indeed, the mitochondria-lysosome contact area of *mcu-1*; *sel-12* mutants was indistinguishable from *sel-12* mutants and larger than wild type animals (Fig. 5A, B). Additionally, *itr-1* RNAi depletion was also unable to rescue the increase in

mitochondria-lysosome contact surface area in *sel-12* mutants (Fig. 5A, C). These data indicate that, despite the impact loss of *mcu-1* or *itr-1* has on lysosome size in *sel-12* mutants, the increased mitochondria-lysosome contacts are not impacted by mitochondria-ER calcium signaling.

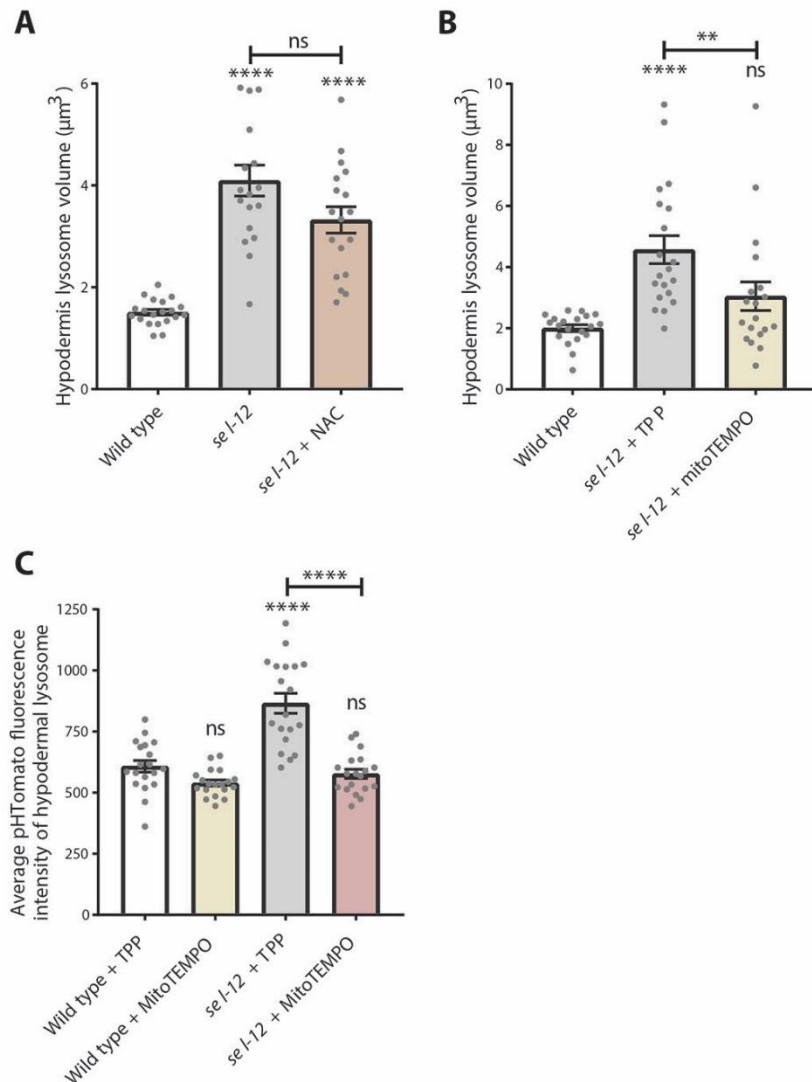


**Figure 7. Lysosome defects are alleviated by mitochondrial-targeted antioxidant treatment.** (A) Lysosome volume (*nuc-1::mCherry*) in wild type, *sel-12(ty11)*, and *sel-12(ty11)* animals grown with N-acetylcysteine (NAC) ( $n \geq 18$  animals). (B) Lysosome volume (*nuc-1::mCherry*) in wild type and *sel-12* animals treated with either the antioxidant MitoTEMPO or vehicle (TPP) ( $n \geq 19$  animals). (C) Quantification of the average pHTomato fluorescence intensity per lysosome in animals expressing *nuc-1::pHTomato* controlled by the heat-shock promoter, with increased pHTomato fluorescence intensity indicating increased pH ( $n \geq 19$  animals). ns  $p > 0.05$ , \* $p < 0.05$ , \*\*\*\* $p < 0.0001$ . For A and C, one-way ANOVA with Tukey's multiple comparisons test was used. For B, Kruskal-Wallis test with Dunn's multiple comparison test was used. Error bars indicate mean  $\pm$  SEM. Comparisons are made to wild type unless otherwise indicated.

We also examined mitochondria-lysosome colocalization in the TRNs by introducing a TRN-specific marker for mitochondria along with the ubiquitous NUC-1::mCherry lysosome reporter. As in the hypodermis, we found increased lysosome-mitochondria contact area in *sel-12* mutants compared to wild type animals (Fig. 5D, E). However, this increase was not affected by inhibiting mitochondrial calcium uptake. Indeed, introduction of the *mcu-1* null mutation into the *sel-12* mutant background did not show a decrease in TRN mitochondria-lysosome contacts (Fig. 5D, E). Altogether, these data suggest that loss of SEL-12 results in increased contact between the

mitochondria and lysosomes, but this is neither influenced by mitochondrial calcium nor ER calcium release, but through an alternate mechanism.

Next, to determine the level of contacts between the ER and the lysosomes, we co-expressed the NUC-1::mCherry lysosomal marker with an ER marker driven under a hypodermal-specific promoter. Similarly, we quantified the contact surface area between the hypodermal ER and lysosomes at a region of interest at the midbody. Like the other inter-organelle interactions, we found increased contact area between the ER and lysosomes in *sel-12* mutants compared to wild type



animals (Fig. 6A, B). Markedly, we found that inhibiting mitochondrial calcium uptake using the *mcu-1* null mutation prevented this increase in contact area between the ER and lysosomes in *sel-12* mutants (Fig. 6A, B). Similarly, inhibiting ER calcium release via *itr-1* RNAi also reduced ER-lysosome contact surface area to wild type levels (Fig. 6A, C). These data indicate that ER calcium release as well as mitochondrial calcium uptake influences ER-lysosome contacts, which may alter ER-lysosome communication and impact lysosome function.

### Lysosome defects are alleviated by mitochondrial-targeted antioxidant treatment

To help understand the mechanism connecting mitochondrial calcium dyshomeostasis and lysosome function in *sel-12* mutants, we explored the impact mitochondrial reactive oxygen species (ROS) have on lysosome function. Previously, we demonstrated that *sel-12* mutants show evidence of elevated oxidative stress [13, 18]. In *sel-12* mutants, increased mitochondrial calcium accumulation disrupts mitochondrial activity and results in increased mitochondrial ROS generation. In agreement with this role of calcium, the elevated ROS in *sel-12* mutants is relieved by inhibiting mitochondrial calcium uptake [13, 18]. Increased mitochondrial ROS may increase the misfolded protein load and put a strain upon the lysosome system and may also explain the connection between mitochondrial calcium and lysosomal defects. Indeed, reducing mitochondrial calcium uptake or ROS production was found to improve proteostasis defects in *sel-12* mutants [17]. To determine the role of oxidative stress in aberrant lysosome morphology, we treated *sel-12* mutants with the antioxidant *n*-acetylcysteine (NAC). However, there was no reduction of lysosome volume with NAC treatment (Fig. 7A). To determine whether specifically targeting mitochondrial ROS would improve lysosome morphology, we treated *sel-12* animals with either MitoTEMPO, which targets the antioxidant piperidine nitroxide (TEMPO) to the mitochondria, or triphenylphosphonium (TPP), the vehicle control. *sel-12* mutants treated with MitoTEMPO showed a significant reduction in lysosome volume compared to *sel-12* mutants treated with TPP (Fig. 7B). Similarly, MitoTEMPO treatment restored *sel-12* mutant lysosome acidity as measured by pHTomato fluorescence intensity (7C). This suggests that mitochondrial ROS, generated by altered ER-to-mitochondria calcium signaling, is responsible for lysosome dysfunction in *sel-12* mutants.

Collectively, these data show that loss of SEL-12 not only promotes interactions between the ER and mitochondria but with the lysosomes as well, which suggests that *sel-12* function is important for regulating

interactions between these three types of organelles. These data may also indicate altered signaling between these organelles in *sel-12* mutants, which in turn impacts their function. Furthermore, we have identified aberrant ER-to-mitochondrial calcium signaling in *sel-12* mutants leads to lysosome morphological and acidification defects by increasing mitochondrial ROS, implicating ER-mitochondrial calcium homeostasis as a factor in lysosome health.

### DISCUSSION

Lysosomal function is necessary for maintaining proteostasis, and its dysfunction is associated with Alzheimer's disease [58, 59]. The phylogenetically conserved protein, presenilin, has been shown to influence lysosome health, but the underlying mechanism is still unclear [10, 14, 20, 22, 24]. In this study, we found that loss of the *C. elegans* presenilin orthologue encoded by the *sel-12* gene disrupts lysosome morphology and function as a result of elevated ER-to-mitochondria calcium signaling. We have identified a novel link between mitochondrial calcium and lysosome health in the context of presenilin function, which may have functional implications into the mechanism underlying fAD. Additionally, this effect is independent of SEL-12's gamma secretase activity, consistent with other studies showing that presenilin loss impacts lysosome function in a gamma secretase-independent manner [10, 11]. Since the activation of lysosomal proteases requires strict maintenance of acidic pH, the morphological changes and increased pH we observed in *sel-12* null mutants likely undermines lysosome overall function and neuronal fitness.

Presenilin's best understood role is acting as the proteolytic subunit of gamma secretase. The gamma secretase complex is required for the proteolytic processing of numerous type I transmembrane domain proteins. Recently, it has been demonstrated that the proteolytic activity of presenilin containing gamma secretase is in acidic compartments, including lysosomes [60]. Thus, the lysosomal morphological changes and functional defects we observe in *sel-12* mutants may arise due to the accumulation of unprocessed membrane proteins. However, this notion is unlikely since we did not observe lysosomal morphology defects in *sel-12* mutants that harbor a mutation that abolishes its proteolytic activity (Supplementary Fig. 1D).

The autophagy-lysosome system is particularly important for neurons, which are mostly post-mitotic and rely on this system to clear intracellular waste and maintain proteome integrity. Indeed, neurons are highly sensitive to insults to lysosome function, as this, for example, will compromise autophagy and lead to a

buildup of damaged, aggregated material. Morphological changes in the lysosome such as enlargement may indicate dysfunction and the accumulation of undigested materials. Lysosomes display significant variation in size to accommodate the contents delivered to them [61]. Enlarged lysosomes might also result from increased lysosome fusion events [16]. Regardless, indicators of morphological and functional lysosome abnormalities presage neuronal damage. Our findings in *sel-12* mutants agree with those in human fAD models which showed enlarged lysosomes [20, 24] and lysosome acidification defects [10, 21, 22], suggesting this important function of presenilin is highly conserved. Indeed, loss of presenilin in *Dictyostelium* also shows defects in lysosome acidification [14]. Considering that *sel-12* mutants show loss of proteostasis [17], it is likely that lysosome dysfunction contributes to proteostatic collapse. Additionally, since lysosome morphological abnormalities occur in L4 animals (the larval stage before adulthood), whereas neuronal defects are first observed in day 1 adults, this suggests that lysosomal defects precede neuronal dysfunction in *sel-12* mutants [13]. Moreover, our data demonstrate the interdependent nature of organelles, as we show that lysosome dysfunction can stem from dysregulated signaling between the ER and mitochondria. Our findings align with a recent study showing that elevated ER calcium release in an AD model resulted in lysosome alkalization and protein aggregation [62]. Furthermore, another recent study found evidence that elevated ER calcium release in an AD mouse model also inhibits autophagy [63]. However, the mechanism underlying these observations is not clear. Here, we implicate mitochondrial calcium and ER-mitochondrial calcium signaling in defective lysosome acidification.

The effect of mitochondrial calcium on lysosome function is unclear. There are studies that demonstrate that ER-mitochondrial calcium dysregulation impacts mitochondrial ROS production and that lysosome calcium levels are affected by increasing mitochondrial ROS, which is generated as a byproduct of increased calcium-mediated mitochondrial activity [64-66]. Mitochondrial dysfunction can alter lysosomal morphology by generating ROS [67]. Presenilin has been shown to interfere with a lysosomal calcium efflux channel, mucolipin transient receptor potential channel subfamily (TRPML1) [22]. Interestingly, TRPML1's function has also been shown to be highly ROS-dependent [68]. In general, lysosomes are susceptible to oxidative stress, and lysosome damage by oxidants sensitizes neurons to apoptosis and necrosis [69]. We have previously demonstrated that ROS generation in *sel-12* mutants results from increased mitochondrial calcium uptake, which triggers neurodegeneration [17, 70]. Here, in *sel-12* mutants, we found that mitochondrial ROS plays a role in

lysosome enlargement and alkalization (Fig. 7B, C). Furthermore, alkalization of lysosomes, which are calcium harboring stores, has been shown to promote calcium efflux [22]. Thus, the lysosome alkalization we observe in *sel-12* mutants likely leads to further defects in calcium homeostasis.

To better understand the relationship between the ER, mitochondria, and lysosomes and how they might influence each other in absence of SEL-12 function, we quantified inter-organelle contact and found increased contact area between all these organelles in *sel-12* null mutants. This suggests that presenilin has an additional role in preventing inappropriate interactions between organelles, perhaps acting as a gatekeeper for inter-organelle communication and signaling in order to maintain cellular homeostasis. Without SEL-12, these interactions are increased, likely resulting in excessive inter-organelle communication. This altered signaling can in turn have downstream consequences on organelle function and impact cellular fitness. There is previous evidence that null or fAD associated presenilin mutations increase ER-mitochondria contact, upregulate membrane protein function at contact sites, and alter lipid and calcium exchange between the ER and mitochondria [8, 46]. Our data show that loss of SEL-12 function also increases contact between the ER and mitochondria in *C. elegans*, which occurs upstream of elevated mitochondrial calcium, as inhibiting mitochondrial calcium uptake was unable to rescue the increase in ER-mitochondrial contact area (Fig. 4A, B). However, we found that knockdown of the ER inositol 1,4,5-trisphosphate receptors suppressed the increased mitochondrial  $\text{Ca}^{2+}$  and ER-mitochondrial contacts observed in *sel-12* mutants (Fig. 4A, C). Importantly, inositol 1,4,5-trisphosphate receptors have been shown to be critical for mediating ER-mitochondrial contact [49-51].

Less is understood about communication between the mitochondria and lysosomes and may be an important understudied relationship influencing neuronal function. Although we found that *sel-12* mutants had increased mitochondrial-lysosome contacts (Fig. 5), the mechanism underlying this aberrant interaction is unclear. There have been studies in other neurodegenerative disease models showing aberrant mitochondria-lysosome contact dynamics that suggest altered communication is involved in disease pathology [71, 72]. Other studies show a close proximity between mitochondria and lysosomes as well as significant crosstalk, especially in regulating calcium homeostasis [73, 74]. Both mitochondria and lysosomes regulate intracellular calcium signaling and are simultaneously influenced by calcium levels [75]. Changes in contact surface area may therefore alter calcium signaling between these two organelles and in turn affect their function. ER-lysosome communication

has been even less studied, although there is data indicating that altering ER-lysosome contact affects neuronal health [76, 77]. It is therefore interesting that our findings demonstrate *sel-12* mutants have increased ER-lysosome contact dependent upon ER-to-mitochondrial calcium signaling (Fig. 6), suggesting another avenue by which altered calcium signaling may influence other organelles and ultimately neuronal health.

Altogether, our study demonstrates a role for ER-to-mitochondrial calcium signaling in lysosome dysfunction caused by loss of SEL-12. SEL-12 loss increases ER-mitochondrial contacts, likely promoting ER-to-mitochondrial calcium exchange, which affects the health of not only the mitochondria but the lysosomes, which in turn likely contributes to proteostatic collapse and neurodegeneration in *sel-12* mutants [13, 17]. The influence of mitochondrial calcium on the lysosomes is also conserved in cells isolated from fAD patients, as we found that inhibiting mitochondrial calcium uptake reduced the enlarged lysosomes observed in fibroblasts isolated from patients harboring fAD mutant presenilin. Additionally, our results indicate that SEL-12 may also be important for regulating inter-organelle contacts and communication between not only the ER and mitochondria but with the lysosome as well. Our data therefore show the importance of inter-organelle crosstalk and how intracellular ER-mitochondrial calcium signaling dysregulates lysosome function in *C. elegans*, providing novel insight into the pathology that may underlie Alzheimer's disease.

### Acknowledgments

We thank Drs. Hannes Buelow, Andrew Chisholm, Oliver Hobert, Natalia Morsci, and Xiaochen Wang, Mei Zhen for sharing reagents and nematode strains. We thank the Caenorhabditis Genetics Center [supported by the National Institutes of Health – Office of Research Infrastructure Programs (P40 OD010440)] and the National Bioresource Project (Tokyo, Japan) for nematode strains. We thank members of the Norman lab for helpful discussion during this project. This work was supported by NIH grants AG064175 and GM145364.

### Supplementary Materials

The Supplementary data can be found online at: [www.aginganddisease.org/EN/10.14336/AD.2024.0228](http://www.aginganddisease.org/EN/10.14336/AD.2024.0228).

### References

- [1] Kaushik S, Cuervo AM (2015). Proteostasis and aging. *Nat Med*, 21: 1406-15.

- [2] Labbadia J, Morimoto RI (2015). The biology of proteostasis in aging and disease. *Annu Rev Biochem*, 84: 435-64.
- [3] Nixon, RA, Yang DS (2011). Autophagy failure in Alzheimer's disease--locating the primary defect. *Neurobiol Dis*, 43: 38-45.
- [4] Wolfe DM, Lee JH, Kumar A, Lee S, Orenstein SJ, Nixon RA (2013). Autophagy failure in Alzheimer's disease and the role of defective lysosomal acidification. *Eur J Neurosci*, 37: 1949-61.
- [5] Boland B, Kumar A, Lee S, Platt FM, Wegiel J, Yu WH, Nixon RA (2008). Autophagy induction and autophagosome clearance in neurons: relationship to autophagic pathology in Alzheimer's disease. *J Neurosci*, 28: 6926-37.
- [6] Yu WH, Cuervo AM, Kumar A, Peterhoff CM, Schmidt SD, Lee JH, Mohan PS, et al. (2005). Macroautophagy--a novel Beta-amyloid peptide-generating pathway activated in Alzheimer's disease. *J Cell Biol*, 171: 87-98.
- [7] Yang DS, Kumar A, Stavrides P, Peterson J, Peterhoff CM, Pawlik M, et al. (2008). Neuronal apoptosis and autophagy cross talk in aging PS/APP mice, a model of Alzheimer's disease. *Am J Pathol*, 173: 665-81.
- [8] Area-Gomez E, Del Carmen Lara Castillo M, Tambini MD, Guardia-Laguarta C, de Groof AJ, Madra M, et al. (2012). Upregulated function of mitochondria-associated ER membranes in Alzheimer disease. *EMBO J*, 31: 4106-23.
- [9] Cheung KH, Shineman D, Müller M, Cárdenas C, Mei L, Yang J, et al. (2008). Mechanism of Ca<sup>2+</sup> disruption in Alzheimer's disease by presenilin regulation of InsP<sub>3</sub> receptor channel gating. *Neuron*, 58: 871-83.
- [10] Lee JH, Yu WH, Kumar A, Lee S, Mohan PS, Peterhoff CM, et al. (2010). Lysosomal proteolysis and autophagy require presenilin 1 and are disrupted by Alzheimer-related PS1 mutations. *Cell*, 141: 1146-58.
- [11] Neely KM, KN Green, LaFerla FM (2011). Presenilin is necessary for efficient proteolysis through the autophagy-lysosome system in a gamma-secretase-independent manner. *J Neurosci*, 31: 2781-91.
- [12] Reddy K, Cusack CL, Nnah IC, Khayati K, Saqena C, Huynh TB, et al. (2016). Dysregulation of Nutrient Sensing and CLEARance in Presenilin Deficiency. *Cell Rep*, 14: 2166-2179.
- [13] Sarasija S, Laboy JT, Ashkavand Z, Bonner J, Tang Y, Norman KR (2018). Presenilin mutations deregulate mitochondrial Ca<sup>2+</sup> homeostasis and metabolic activity causing neurodegeneration in *Caenorhabditis elegans*. *Elife*, 7: e33052.
- [14] Sharma D, Otto G, Warren EC, Beesley P, King JS, Williams RSB (2019). Gamma secretase orthologs are required for lysosomal activity and autophagic degradation in *Dictyostelium discoideum*, independent of PSEN (presenilin) proteolytic function. *Autophagy*, 15: 1407-1418.
- [15] Tu H, Nelson O, Bezprozvanny A, Wang Z, Lee SF, Hao YH, et al. (2006). Presenilins form ER Ca<sup>2+</sup> leak channels, a function disrupted by familial Alzheimer's disease-linked mutations. *Cell*, 126: 981-93.

- [16] Orr ME, Oddo S (2013). Autophagic/lysosomal dysfunction in Alzheimer's disease. *Alzheimers Res Ther*, 5: 53.
- [17] Ashkavand Z, Sarasija S, Ryan KC, Laboy JT, Norman KR (2020). Corrupted ER-mitochondrial calcium homeostasis promotes the collapse of proteostasis. *Aging Cell*, 19: e13065.
- [18] Ryan KC, Ashkavand Z, Sarasija S, Laboy JT, Samarakoon R, Norman KR (2021). Increased Mitochondrial Calcium Uptake and Concomitant Hyperactivity by Presenilin Loss Promotes mTORC1 Signaling to Drive Neurodegeneration. *Aging Cell*, 19: e13065.
- [19] Neely Kayala KM, Dickinson GD, Minassian A, Walls KC, Green KN, Laferla FM (2012). Presenilin-null cells have altered two-pore calcium channel expression and lysosomal calcium: implications for lysosomal function. *Brain Res*, 1489: 8-16.
- [20] Coen K, Flannagan RS, Baron S, Carraro-Lacroix LR, Wang D, Vermeire W, et al. (2012). Lysosomal calcium homeostasis defects, not proton pump defects, cause endo-lysosomal dysfunction in PSEN-deficient cells. *J Cell Biol*, 198: 23-35.
- [21] Coffey EE, Beckel JM, Laties AM, Mitchell CH (2014). Lysosomal alkalization and dysfunction in human fibroblasts with the Alzheimer's disease-linked presenilin 1 A246E mutation can be reversed with cAMP. *Neuroscience*, 263: 111-24.
- [22] Lee JH, McBrayer MK, Wolfe DM, Haslett LJ, Kumar A, Sato Y, et al. (2015). Presenilin 1 Maintains Lysosomal Ca(2+) Homeostasis via TRPML1 by Regulating vATPase-Mediated Lysosome Acidification. *Cell Rep*, 12: 1430-44.
- [23] Nixon RA, Wegiel J, Kumar A, Yu WH, Peterhoff C, Cataldo A, et al. (2005). Extensive involvement of autophagy in Alzheimer disease: an immuno-electron microscopy study. *J Neuropathol Exp Neurol*, 64: 113-22.
- [24] Hung COY, Livesey, FJ (2018). Altered gamma-Secretase Processing of APP Disrupts Lysosome and Autophagosome Function in Monogenic Alzheimer's Disease. *Cell Rep*, 25: 3647-3660 e2.
- [25] Lee JH, Yang DS, Goulbourne CN, Im E, Stavrides P, Pensalfini A, et al. (2022). Faulty autolysosome acidification in Alzheimer's disease mouse models induces autophagic build-up of Abeta in neurons, yielding senile plaques. *Nat Neurosci*, 25: 688-701.
- [26] Mello CC, Kramer JM, Stinchcomb D, Ambros V. (1991). Efficient gene transfer in C.elegans: extrachromosomal maintenance and integration of transforming sequences. *EMBO J*, 10: 3959-70.
- [27] Timmons L, Fire A (1998). Specific interference by ingested dsRNA. *Nature*, 395: 854.
- [28] Kamath RS, Fraser AG, Dong Y, Poulin G, Durbin R, Gotta M, et al. (2003). Systematic functional analysis of the *Caenorhabditis elegans* genome using RNAi. *Nature*, 421: 231-7.
- [29] Sun Y, Li M, Zhao D, Li X, Yang C, Wang X (2020). Lysosome activity is modulated by multiple longevity pathways and is important for lifespan extension in *C. elegans*. *Elife*, 9: e55745.
- [30] Wang L, Goldwag J, Bouyea M, Barra J, Matteson K, Maharjan N, et al. (2023). Spatial topology of organelle is a new breast cancer cell classifier. *iScience*, 26: 107229.
- [31] Tank EM, Rodgers KE, Kenyon C (2011). Spontaneous age-related neurite branching in *Caenorhabditis elegans*. *J Neurosci*, 31: 9279-88.
- [32] Toth ML, Melentijevic I, Shah L, Bhatia A, Lu K, Talwar A, et al. (2012). Neurite sprouting and synapse deterioration in the aging *Caenorhabditis elegans* nervous system. *J Neurosci*, 32: 8778-90.
- [33] Clark SG, Chiu C (2003). *C. elegans* ZAG-1, a Zn-finger-homeodomain protein, regulates axonal development and neuronal differentiation. *Development*, 130: 3781-94.
- [34] Guo P, Hu T, Zhang J, Jiang S, Wang X (2010). Sequential action of *Caenorhabditis elegans* Rab GTPases regulates phagolysosome formation during apoptotic cell degradation. *Proc Natl Acad Sci U S A*, 107: 18016-21.
- [35] Cinar HN, Sweet KL, Hosemann KE, Earley K, Newman AP (2001). The SEL-12 presenilin mediates induction of the *Caenorhabditis elegans* uterine pi cell fate. *Dev Biol*, 237: 173-82.
- [36] Levitan D, Greenwald I (1995). Facilitation of lin-12-mediated signalling by sel-12, a *Caenorhabditis elegans* S182 Alzheimer's disease gene. *Nature*, 377: 351-4.
- [37] El Mouridi S, Lecroisey C, Tardy P, Mercier M, Leclercq-Blondel A, Zariohi N, et al. Reliable CRISPR/Cas9 Genome Engineering in *Caenorhabditis elegans* Using a Single Efficient sgRNA and an Easily Recognizable Phenotype. *G3 (Bethesda)*, 7: 1429-1437.
- [38] Li Y, Tsien RW (2012). pHTomato, a red, genetically encoded indicator that enables multiplex interrogation of synaptic activity. *Nat Neurosci*, 15: 1047-53.
- [39] Chou CC, Vest R, Prado MA, Wilson-Grady J, Paulo JA, Shibuya Y, Moran-Losada P, et al. (2023). Proteostasis and lysosomal quality control deficits in Alzheimer's disease neurons. *bioRxiv*, 2023.03.27.534444.
- [40] Xu S, Chisholm AD (2014). *C. elegans* epidermal wounding induces a mitochondrial ROS burst that promotes wound repair. *Dev Cell*, 31: 48-60.
- [41] Álvarez-Illera P, García-Casas P, Fonteriz RI, Montero M, Alvarez J (2020). Mitochondrial Ca(2+) Dynamics in MCU Knockout *C. elegans* Worms. *Int J Mol Sci*, 21: 8622.
- [42] Lee SY, Hwang DY, Kim YK, Lee JW, Shin IC, Oh KW, et al. (2006). PS2 mutation increases neuronal cell vulnerability to neurotoxins through activation of caspase-3 by enhancing of ryanodine receptor-mediated calcium release. *FASEB J*, 20: 151-3.
- [43] Green KN, Demuro A, Akbari Y, Hitt BD, Smith IF, Parker I, et al. (2008). SERCA pump activity is physiologically regulated by presenilin and regulates amyloid beta production. *J Cell Biol*, 181: 1107-16.
- [44] Popugaeva E, Pchitskaya E, Bezprozvanny I (2017). Dysregulation of neuronal calcium homeostasis in



- Alzheimer's disease - A therapeutic opportunity? *Biochem Biophys Res Commun*, 483: 998-1004.
- [45] Hedskog L, Pinho CM, Filadi R, Rönnbäck A, Hertwig L, Wiehager B, et al. (2013). Modulation of the endoplasmic reticulum-mitochondria interface in Alzheimer's disease and related models. *Proc Natl Acad Sci U S A*, 110: 7916-21.
- [46] Zampese, E., et al., Presenilin 2 modulates endoplasmic reticulum (ER)-mitochondria interactions and Ca<sup>2+</sup> cross-talk. *Proc Natl Acad Sci U S A*, 2011. 108(7): p. 2777-82.
- [47] Area-Gomez E, de Groof AJ, Boldogh I, Bird TD, Gibson GE, Koehler CM, et al. (2009). Presenilins are enriched in endoplasmic reticulum membranes associated with mitochondria. *Am J Pathol*, 175: 1810-6.
- [48] Area-Gomez E, Schon EA (2017). On the Pathogenesis of Alzheimer's Disease: The MAM Hypothesis. *FASEB J*, 31: 864-867.
- [49] Xie L, Gao S, Alcaire SM, Aoyagi K, Wang Y, Griffin JK, et al. (2013). NLF-1 delivers a sodium leak channel to regulate neuronal excitability and modulate rhythmic locomotion. *Neuron*, 77: 1069-82.
- [50] Levitan D, Greenwald I (1998). Effects of SEL-12 presenilin on LIN-12 localization and function in *Caenorhabditis elegans*. *Development*, 125: 3599-606.
- [51] Xu S, Wang Z, Kim KW, Jin Y, Chisholm AD (2016). Targeted Mutagenesis of Duplicated Genes in *Caenorhabditis elegans* Using CRISPR-Cas9. *J Genet Genomics*, 43: 103-6.
- [52] Szabadkai G, Bianchi K, Várnai P, De Stefani D, Wieckowski MR, Cavagna D, et al. (2006). Chaperone-mediated coupling of endoplasmic reticulum and mitochondrial Ca<sup>2+</sup> channels. *J Cell Biol*, 175: 901-11.
- [53] Csordas G, Weaver D, Hajnóczky G (2018). Endoplasmic Reticulum-Mitochondrial Contactology: Structure and Signaling Functions. *Trends Cell Biol*, 28: 523-540.
- [54] Bartok A, Weaver D, Golenár T, Nichtova Z, Katona M, Bánsághi S, et al. (2019). IP(3) receptor isoforms differently regulate ER-mitochondrial contacts and local calcium transfer. *Nat Commun*, 10: 3726.
- [55] Pasternak SH, Bagshaw RD, Guiral M, Zhang S, Ackerley CA, Pak BJ, et al. (2003). Presenilin-1, nicastrin, amyloid precursor protein, and gamma-secretase activity are co-localized in the lysosomal membrane. *J Biol Chem*, 278: 26687-94.
- [56] Sannerud R, Esselens C, Ejsmont P, Mattera R, Rochin L, Tharkeshwar AK, et al. (2016). Restricted Location of PSEN2/gamma-Secretase Determines Substrate Specificity and Generates an Intracellular Abeta Pool. *Cell*, 166: 193-208.
- [57] Li Y, Chen B, Zou W, Wang X, Wu Y, Zhao D, et al. The lysosomal membrane protein SCAV-3 maintains lysosome integrity and adult longevity. *J Cell Biol*, 215: 167-185.
- [58] Bonam SR, Wang F, Muller S (2019). Lysosomes as a therapeutic target. *Nat Rev Drug Discov*, 18: 923-948.
- [59] Zhang L, Sheng R, Qin Z (2009). The lysosome and neurodegenerative diseases. *Acta Biochim Biophys Sin (Shanghai)*, 41: 437-45.
- [60] Maesako M, Houser MCQ, Turchyna Y, Wolfe MS, Berezovska O (2022). Presenilin/gamma-Secretase Activity Is Located in Acidic Compartments of Live Neurons. *J Neurosci*, 42: 145-154.
- [61] de Araujo MEG, Liebscher G, Hess MW, Huber LA (2020). Lysosomal size matters. *Traffic*, 21: 60-75.
- [62] Mustaly-Kalimi S, Gallegos W, Marr RA, Gilman-Sachs A, Peterson DA, Sekler I, et al. (2022). Protein mishandling and impaired lysosomal proteolysis generated through calcium dysregulation in Alzheimer's disease. *Proc Natl Acad Sci U S A*, 119: e2211999119.
- [63] Zhang H, Knight C, Chen SRW, Bezprozvanny I (2023). A Gating Mutation in Ryanodine Receptor Type 2 Rescues Phenotypes of Alzheimer's Disease Mouse Models by Upregulating Neuronal Autophagy. *J Neurosci*, 43: 1441-1454.
- [64] Booth DM, Enyedi B, Geiszt M, Várnai P, Hajnóczky G (2016). Redox Nanodomains Are Induced by and Control Calcium Signaling at the ER-Mitochondrial Interface. *Mol Cell*, 63: 240-248.
- [65] Song SB, Hwang ES (2020). High Levels of ROS Impair Lysosomal Acidity and Autophagy Flux in Glucose-Deprived Fibroblasts by Activating ATM and Erk Pathways. *Biomolecules*, 10: 761.
- [66] Yuan Y, Chen Y, Peng T, Li L, Zhu W, Liu F, et al. (2019). Mitochondrial ROS-induced lysosomal dysfunction impairs autophagic flux and contributes to M1 macrophage polarization in a diabetic condition. *Clin Sci (Lond)*, 133: 1759-1777.
- [67] Demers-Lamarche J, Guillebaud G, Tlili M, Todkar K, Bélanger N, Grondin M, et al. (2016). Loss of Mitochondrial Function Impairs Lysosomes. *J Biol Chem*, 291: 10263-76.
- [68] Zhang X, Cheng X, Yu L, Yang J, Calvo R, Patnaik S, et al. (2016). MCOLN1 is a ROS sensor in lysosomes that regulates autophagy. *Nat Commun*, 7: 12109.
- [69] Pivtoraiko VN, Stone SL, Roth KA, Shacka JJ (2009). Oxidative stress and autophagy in the regulation of lysosome-dependent neuron death. *Antioxid Redox Signal*, 11: 481-96.
- [70] Ryan KC, Laboy JT, Norman KR (2022). Deregulation of Mitochondrial Calcium Handling Due to Presenilin Loss Disrupts Redox Homeostasis and Promotes Neuronal Dysfunction. *Antioxidants (Basel)*, 11: 1642.
- [71] Höglinger D, Burgoyne T, Sanchez-Heras E, Hartwig P, Colaco A, Newton J, et al. (2019). NPC1 regulates ER contacts with endocytic organelles to mediate cholesterol egress. *Nat Commun*, 10: 4276.
- [72] Cisneros J, Belton TB, Shum GC, Molakal CG, Wong YC (2022). Mitochondria-lysosome contact site dynamics and misregulation in neurodegenerative diseases. *Trends Neurosci*, 45: 312-322.
- [73] Wong YC, Kim S, Peng W, Krainc D. (2019). Regulation and Function of Mitochondria-Lysosome Membrane Contact Sites in Cellular Homeostasis. *Trends Cell Biol*, 29: 500-513.
- [74] Peng W, Wong YC, Krainc D (2020). Mitochondria-lysosome contacts regulate mitochondrial Ca(2+) dynamics via lysosomal TRPML1. *Proc Natl Acad Sci U S A*, 117: 19266-19275.

- [75] Feng X, Yang J (2016). Lysosomal Calcium in Neurodegeneration. *Messenger (Los Angel)*, 5: 56-66.
- [76] Özkan N, Koppers M, van Soest I, van Harten A, Jurriens D, Liv N, et al. (2021). ER - lysosome contacts at a pre-axonal region regulate axonal lysosome availability. *Nat Commun*, 12: 4493.
- [77] Lu M, van Tartwijk FW, Lin JQ, Nijenhuis W, Parutto P, Fantham M, et al. (2020). The structure and global distribution of the endoplasmic reticulum network are actively regulated by lysosomes. *Sci Adv*, 6: eabc7209.